Biophysical Journal
Biophysical Perspective

Biophysical Society

Genetically Encoded Fluorescent Indicators for Organellar Calcium Imaging

Junji Suzuki,[1,2] Kazunori Kanemaru,[1] and Masamitsu Iino[1,3,*]
[1]Department of Pharmacology, Graduate School of Medicine, The University of Tokyo, Tokyo, Japan; [2]Department of Physiology, University of California San Francisco, San Francisco, California; and [3]Department of Cellular and Molecular Pharmacology, Nihon University School of Medicine, Tokyo, Japan

ABSTRACT Optical Ca^{2+} indicators are powerful tools for investigating intracellular Ca^{2+} signals in living cells. Although a variety of Ca^{2+} indicators have been developed, deciphering the physiological functions and spatiotemporal dynamics of Ca^{2+} in intracellular organelles remains challenging. Genetically encoded Ca^{2+} indicators (GECIs) using fluorescent proteins are promising tools for organellar Ca^{2+} imaging, and much effort has been devoted to their development. In this review, we first discuss the key points of organellar Ca^{2+} imaging and summarize the requirements for optimal organellar Ca^{2+} indicators. Then, we highlight some of the recent advances in the engineering of fluorescent GECIs targeted to specific organelles. Finally, we discuss the limitations of currently available GECIs and the requirements for advancing the research on intraorganellar Ca^{2+} signaling.

Ca^{2+} is an important second messenger that regulates numerous physiological cellular functions (1). The versatility of intracellular Ca^{2+} signaling relies on the precise control of spatiotemporal Ca^{2+} dynamics (2). Intracellular organelles play a pivotal role in generating Ca^{2+} signaling patterns by acting as sinks and sources of Ca^{2+}. Furthermore, intraorganellar Ca^{2+} concentrations regulate the activities of enzymes residing in each organelle, and disturbances in organellar Ca^{2+} signaling are implicated in various pathophysiological conditions (3,4). Thus, investigations into organellar Ca^{2+} dynamics are indispensable for advancing our understanding of the role of intracellular Ca^{2+} signals in cell physiology and pathophysiology. Optical Ca^{2+} indicators, which alter their spectral properties depending on the surrounding Ca^{2+} concentration, are useful tools for the quantitative analysis of organellar Ca^{2+} signals in living organisms.

Ideally, organellar Ca^{2+} indicators should fulfill the following requirements. First, they should localize specifically in the target organelle. Second, they should exhibit strong fluorescence, high signal/noise, and fast kinetics, sufficient to resolve the spatial and temporal dynamics of organellar Ca^{2+} signals. Third, they should possess affinity for Ca^{2+} suitable for detecting changes in Ca^{2+} concentration in the target organelle, because the range of intraorganellar Ca^{2+} concentrations can vary from nanomolar to submillimolar (see Fig. 1). Furthermore, it is desirable that they exhibit a monophasic Ca^{2+} titration curve, so that the fluorescence intensity changes are proportionally converted to Ca^{2+} concentration changes. Fourth, their signals should not be disturbed by organelle-specific environmental factors such as acidic or basic pH, because organelles have unique environments optimized for their functions. Fifth, a frequent requirement is noninterference with the measurement of other fluorescent molecules that may be used simultaneously. Last, the indicators should not be toxic to cells. In the light of these requirements, a wide variety of organellar Ca^{2+} indicators have been developed.

Small molecular fluorescent Ca^{2+} indicators have been used for Ca^{2+} imaging in several organelles. For example, furaptra and rhod-2 have been used for Ca^{2+} imaging in the sarco/endoplasmic reticulum (SR/ER) and mitochondria, respectively (5). These dyes are easily loaded into the intracellular space by using their acetoxymethyl esters, enabling imaging with high spatiotemporal resolution. However, these indicators face a drawback in that they cannot be selectively localized in the desired organelle; they are instead inevitably retained in the cytoplasm. Therefore, organellar Ca^{2+} imaging cannot be performed before the excess cytosolic indicator molecules are removed either by dialysis through a micropipette or by permeabilization of the plasma membrane. These procedures may preclude organellar Ca^{2+} imaging under physiological conditions. Furthermore, it is also difficult to use these dyes for long-term imaging, because they leak out of the organelles in a time-dependent manner.

The development of genetically encoded Ca^{2+} indicators (GECIs) is expected to lift the constraints associated with

Submitted November 18, 2015, and accepted for publication April 1, 2016.
*Correspondence: iino@m.u-tokyo.ac.jp
Editor: Mark Cannell.
http://dx.doi.org/10.1016/j.bpj.2016.04.054

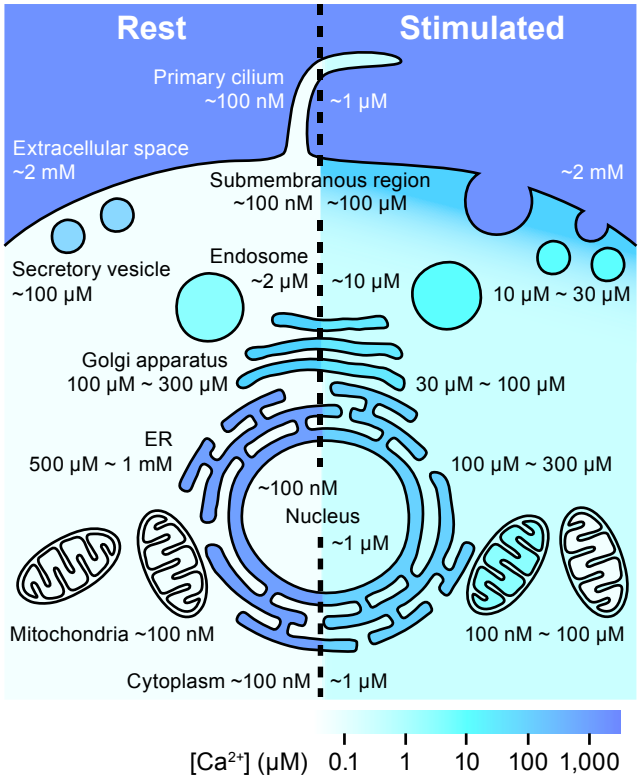

FIGURE 1 Ca^{2+} concentrations in subcellular compartments. Ca^{2+} concentrations in the intracellular organelles and subcellular compartments in the resting state (*left*) and after stimulation (*right*). This represents a summary of the results obtained to date using the organellar genetically encoded Ca^{2+} indicators reviewed here. To see this figure in color, go online.

small molecular Ca^{2+} indicators, because GECIs can be selectively expressed and retained in organelles by fusing organelle-specific targeting sequences to the indicator molecule. The first organelle-targeted GECI was engineered using aequorin, a Ca^{2+}-sensitive bioluminescent protein (LP), which emits light via enzymatic reaction in the presence of both Ca^{2+} and the cofactor coelenterazine (6,7). Aequorin derivatives have been successfully used for detecting Ca^{2+} dynamics with a high signal/noise in several organelles including the ER, mitochondria, nucleus, Golgi apparatus, plasma membrane, peroxisomes, and secretory vesicles (8). Because excitation illumination is not required for their observation, their measurements are free from autofluorescence or phototoxicity. However, their low photon emission rate makes it difficult to obtain subcellular resolution. In addition, the irreversible nature of the luminescence limits the duration of measurements.

GECIs based on fluorescent proteins (FPs) have opened up a new era in organellar Ca^{2+} imaging. FP-based GECIs have several advantages over the LP-based indicators; they are bright enough to visualize Ca^{2+} dynamics with subcellular resolution, and their reaction is reversible and does not require any cofactors. Thus, fluorescent GECIs have properties suitable for quantitative measurements of organellar Ca^{2+} signals. In general, FP-based GECIs are categorized into two classes: dual-FP type and single-FP type. The dual-FP type GECIs, which comprise two FPs linked by a Ca^{2+}-responsive element, are founded on the principle of Förster resonance energy transfer (FRET), a process whereby energy liberated from the donor FP is transferred to the neighboring acceptor FP. The efficiency of FRET depends on the donor-acceptor distance and orientation as well as the spectral overlap between the donor emission and the acceptor excitation. Ca^{2+} binding to the Ca^{2+}-responsive element causes a conformational change in the indicator, which alters the FRET efficiency between the two FPs. This results in a change in fluorescence intensity of both donor and acceptor FPs, enabling ratiometric measurements. The first and most widely used FRET-type GECI was cameleon, which consists of cyan and yellow FPs as the donor and acceptor, respectively, linked by calmodulin (CaM) and the M13 peptide from the myosin light-chain kinase (9). Derivative indicators of cameleon have been used for Ca^{2+} imaging in a variety of organelles including the ER, mitochondrial inner matrix, mitochondrial outer membrane, Golgi apparatus, nucleus, secretory granules, plasma membrane, and peroxisomes (9–18).

The single-FP-type GECIs are made up of circularly permutated FP and a Ca^{2+}-responsive element. Ca^{2+}-dependent conformational change of the indicators alters the protonation state of the fluorophores of the FPs, resulting in a change in fluorescent intensity. The advantages of single-FP-type GECIs compared with the FRET types are that they generally have a higher dynamic range and use a relatively narrower range of excitation and emission wavelengths, which makes it easy to perform simultaneous imaging with other fluorescent molecules. Although most of these indicators allow only intensiometric Ca^{2+} measurements because they contain only one FP, certain single-FP indicators can be used for ratiometric imaging (19–22). The single-FP GECIs have been used for Ca^{2+} imaging in various organelles including the ER, ER membrane, mitochondrial inner matrix, mitochondrial outer membrane, Golgi apparatus, endosomes, nucleus, plasma membrane, and primary cilia (11,19,21,23–30).

As described above, a large variety of organellar Ca^{2+} indicators have been developed. In the following sections, we review the design strategies and properties of fluorescent GECIs for each target organelle. A list of organellar GECIs discussed in this review is provided in Table 1, along with their respective characteristics. Intraorganellar Ca^{2+} concentrations obtained with the organellar GECIs reviewed here are summarized in Fig. 1.

Sarco/endoplasmic reticulum

The SR/ER accumulates Ca^{2+} in its luminal space and acts as a major source of Ca^{2+} for generating intracellular Ca^{2+} signals. Indeed, Ca^{2+} release from the SR/ER increases

cytosolic Ca^{2+} concentrations both in excitable and nonexcitable cells, and it also regulates a variety of cell functions, such as contraction, fertilization, development, vesicular secretion, and synaptic plasticity (1). Furthermore, the Ca^{2+} level within the ER is an important factor in ER function because ER-residing chaperones require Ca^{2+} for their activities (31). In contrast, Ca^{2+} depletion of the ER triggers ER stress through the accumulation of misfolded proteins, causing apoptosis (3). Consequently, much effort has been devoted to the development of GECIs for visualizing ER Ca^{2+} dynamics.

To achieve selective localization of GECIs in the lumen of the ER, an ER-targeting sequence and the ER retention signal KDEL were attached to the N- and C-terminus of the GECIs, respectively. A high value of apparent dissociation constant (K_d) is a critical factor for ER GECIs because free Ca^{2+} concentrations in the ER lumen may reach the submillimolar range, which is ~10,000 times higher than that in the cytoplasm (Fig. 1). Introduction of mutations in the Ca^{2+}-responsive element of the cytosolic GECIs has been used to increase the K_d value, but such alterations often have an adverse effect in decreasing the dynamic range of these indicators. Several strategies have been employed to optimize these contradictory effects, such as substituting multiple amino acids in the Ca^{2+}-binding sites, using Ca^{2+}-responsive elements derived from endogenous ER-residing Ca^{2+}-binding proteins, and designing artificial Ca^{2+}-binding sites (12,23–25,32–34).

The first fluorescent ER GECIs to be developed were the cameleon-type indicators, YC3er and YC4er (9). To lower the Ca^{2+} affinity of their parent GECI, YC2, YC3er, and YC4er contain point mutations in the Ca^{2+}-binding sites of CaM within the indicator molecule. YC3er has a K_d of 4.4 μM, which is too low to faithfully report the entire range of ER Ca^{2+} dynamics. YC4er has a biphasic Ca^{2+} titration curve with K_d values of 0.083 and 700 μM, the higher of which is sufficient to detect ER Ca^{2+} dynamics, but with a limited dynamic range. YC4er was subsequently improved to generate D1ER by redesigning the binding interface between CaM and M13 to minimize nonspecific interactions with endogenous CaM (12), although it also has a biphasic Ca^{2+} titration curve (K_d = 0.81 and 60 μM). Further improvements have led to the generation of low-affinity variants such as D4ER (K_d = 195 μM) and split-YC7.3er (K_d = 130 μM), and a red-shifted variant named D1ERCmR2, by substituting CFP and YFP with Clover and mRuby FPs, respectively (35–37). In parallel with these improvements of the cameleon-type GECIs, a unique FRET-type ER GECI named "apoK1er" has been developed (34). Instead of CaM and M13, apoK1er employs a kringle domain as the Ca^{2+}-responsive element, which is derived from apolipoprotein A and shifts from a linear form to a compact structure via the Ca^{2+}-dependent activities of ER-resident chaperones. This approach has the advantage that Ca^{2+} buffering within the ER is not affected by the expression of the Ca^{2+} indicator because apoK1er itself does not bind Ca^{2+}. However, it also has the disadvantage that the indicator is sensitive not only to Ca^{2+}, but also to the redox state of the ER.

In addition to these FRET-type ER GECIs, several types of single-FP ER GECIs have been developed. The first report of such indicators is Ca-G1-ER, which was created by grafting a Ca^{2+}-binding motif from CaM into fluorophore-sensitive locations in EGFP (33). Ca-G1-ER has a low sensitivity toward Ca^{2+} with a K_d of ~600–800 μM. Ca^{2+} binding to Ca-G1-ER results in an increase in fluorescence with excitation at 398 nm and a decrease with excitation at 490 nm. The ratio of the fluorescence intensity at these two excitation wavelengths increases by 80% upon Ca^{2+} binding. Later, the same research group developed CatchER, which also has a Ca^{2+}-binding site introduced near the fluorophore in EGFP. The Ca^{2+}-binding site was created by introducing point mutations instead of CaM grafting (23). CatchER has a K_d of 180 μM, fast kinetics, and a dynamic range value of 230%.

A recent entry to this category is a family of CEPIAs (24), generated on the basis of single-FP-based cytosolic GECIs (GECOs) (20). CEPIA indicators were generated by introducing point mutations in the Ca^{2+}-binding domains of CaM of GECOs, and have low Ca^{2+} affinities (K_d = 500–700 μM) favorable for detecting ER Ca^{2+} dynamics. CEPIAs have three unique features. First, CEPIAs have three color variants, G-CEPIA1*er* (*green*), R-CEPIA1*er* (*red*), and GEM-CEPIA1*er* (*blue* and *green*), utilizing the color palette of GECOs. Second, they have high signal/noise and large dynamic ranges (470–2100%), enabling visualization of ER Ca^{2+} dynamics with subcellular resolution such that wavelike Ca^{2+} release from the ER could be visualized for the first time (Fig. 2) (24). Third, they allow the simultaneous use of other indicators, enabling multiparametric measurements such as simultaneous Ca^{2+} imaging in three subcellular compartments, i.e., the ER, mitochondria, and cytosol (Fig. 3) (24). Owing to these characteristics, CEPIAs have been successfully used to shed new light on ER Ca^{2+} dynamics, such as the importance of Ca^{2+} diffusion within the ER (Ca^{2+} tunneling) for the replenishment of ER Ca^{2+} after synaptic inputs in cerebellar Purkinje cells (38), and abnormal ER Ca^{2+} handling associated with disease-related mutations of the ryanodine receptor Ca^{2+} release channel (39). Other groups also reported ER GECIs based on GECO or its analog GCaMP3. ER-LAR-GECO1 was generated by combining the strategies of random and site-directed mutagenesis of the CaM-M13 interaction sites in R-GECO1, resulting in a K_d of 24 μM and a dynamic range of 1000% (25). GCaMPer (10.19) was created by introducing multiple mutations in the Ca^{2+}-binding sites of GCaMP3, yielding a K_d of 400 μM and a dynamic range of 1400% (32).

Another entry to the ER GECIs is erGAP1, which is a derivative of GAP, a fusion protein of aequorin and GFP (21).

TABLE 1 Properties of Fluorescent GECIs for Organelles

Locus	Name	Type[a]	Tag	K_d for Ca^{2+}	Dynamic range	Hill coefficient	pK_a (Ca^{2+} ±)	Ca^{2+}-responsive elements	Fluorophore	Excitation peak (nm)	Emission peak (nm)	Reference
ER	YC3er	FRET	Calreticulin, KDEL	4.4 μM	—	0.76	—	CaM, M13	ECFP, EYFP	433	475, 527	(9)
	YC4er	FRET	Calreticulin, KDEL	0.083, 700 μM	—	1.5, 0.87	—	CaM, M13	ECFP, EYFP	433	475, 527	(9)
	YC3.3er	FRET	Calreticulin, KDEL	—	—	—	—	CaM, M13	ECFP, Citrine	433	475, 529	(11)
	D1ER	FRET	Calreticulin, KDEL	0.081, 60 μM	—	1.18, 1.67	—	CaM, M13	ECFP, Citrine	433	475, 529	(12)
	split-YC7.3er	FRET	Calreticulin, KDEL	130 μM	—	1.4	—	CaM, M13	ECFP, Citrine	433	475, 529	(35)
	D4ER	FRET	Calreticulin, KDEL	195 μM	—	—	—	CaM, M13	ECFP, Citrine	433	475, 529	(36)
	mTFP1-YC3.3	FRET	Calreticulin, KDEL	—	—	—	—	CaM, M13	mTFP1, Citrine	462	492, 529	(89)
	D1ERCmR2	FRET	Calreticulin, KDEL	200 μM	—	0.5	—	CaM, M13	Clover, mRuby2	490	510, 560	(37)
	T1ER	FRET	Calreticulin, KDEL	—	—	—	—	CaM, M13	mTurquoise, Citrine	434	474, 529	(90)
	apoK1-er	FRET	Calreticulin, KDEL	124 μM	—	1.2	—	kringle	ECFP, EYFP	433	475, 527	(34)
	G-CEPIA1er	Intensio	Immunoglobulin Vh, KDEL	672 μM	4.7	1.95	8.0/8.7	CaM, M13	cpEGFP	497	511	(24)
	R-CEPIA1er	Intensio	Immunoglobulin Vh, KDEL	565 μM	8.8	1.7	6.5, 9.0/8.9	CaM, M13	cpmApple	562	584	(24)
	GEM-CEPIA1er	Ratio	Immunoglobulin Vh, KDEL	558 μM	21.7	1.37	6.5, 10.6/6.1	CaM, M13	cpEGFP	391	462, 510	(24)
	ER-LAR-GECO1	Intensio	Calreticulin, KDEL	24 μM	10	1.3	5.4, 8.8/8.6	CaM, M13	cpmApple	561	589	(25)
	GCaMPer(10.19)	Intensio	Calreticulin, KDEL	400 μM	14	1.9	7.2/8.0	CaM, M13	cpEGFP	496	513	(32)
	Ca-G1-ER	Ratio	Calreticulin, KDEL	800 μM	1.8	1	7.45	Graft Ca^{2+} binding site	EGFP	398, 490	510	(33)
	CatchER	Intensio	Calreticulin, KDEL	180 μM	2.3	0.94	6.91/7.59	Create Ca^{2+} binding site	EGFP	398, 490	510	(23)
	erGAP1	Ratio	Calreticulin, KDEL	12 μM	2.7	1	—	Aequorin	GFP, Aequorin	403, 470	510	(21)
ER membrane	GCaMP6f-T/J	Intensio	Triadin or junctin 1	375 nM	51.8	2.27	6.34/8.77	CaM, M13	cpEGFP	497	515	(29)
Golgi apparatus	GT-YC3.3	FRET	N81 of galactosyltransferase type II	1.5 μM	—	—	—	CaM, M13	ECFP, Citrine	433	475, 529	(11)
	Go-D1cpv	FRET	N69 of sialyl-transferase I	—	—	—	—	CaM, M13	ECFP, Citrine	433	475, 529	(42)
	medialGo-D1cpv	FRET	N32 of N-acetylglucosaminyl transferase	27.4 μM	—	—	—	CaM, M13	ECFP, Citrine	433	475, 529	(43)
	goGAP1	Ratio	N81 of galactosyltransferase type II	12 μM	—	1	—	Aequorin	GFP variant, Aequorin	403, 470	510	(21)
Secretory granules	D1-SG	FRET	tPA	0.081, 60 μM	—	—	—	CaM, M13	ECFP, Citrine	433	475, 529	(17)
Endosomes	TiVAMP-GEM-GECO1	Ratio	C61 of TiVAMP	340 nM	110	2.94	6.16	CaM, M13	cpEGFP	390	455, 510	(27)
Mitochondria	YC2mt	FRET	1× COX VIII	1.24 μM	—	0.79	—	CaM, M13	EGFP, EYFP	433	475, 527	(10)
	YC2.1mt	FRET	1× COX VIII	—	—	—	—	CaM, M13	EGFP, EYFP variant	433	475, 527	(10)
	YC3.1mt	FRET	1× COX VIII	3.98 μM	—	—	—	CaM, M13	EGFP, EYFP variant	433	475, 527	(10)
	YC4.1mt	FRET	1× COX VIII	0.105, 104 μM	—	—	—	CaM, M13	EGFP, EYFP variant	433	475, 527	(10)
	2mt8YC2	FRET	2× COX VIII	1.24 μM	—	—	—	CaM, M13	EGFP, EYFP	433	475, 527	(13)
	2mt8YC2.1	FRET	2× COX VIII	1.24 μM	—	—	—	CaM, M13	EGFP, EYFP variant	433	475, 527	(13)
	2mt8YC2.12	FRET	2× COX VIII	1.24 μM	—	—	—	CaM, M13	EGFP, EYFP variant	433	475, 527	(13)

(Continued on next page)

Table 1. *Continued*

Locus	Name	Type[a]	Tag	K_d for Ca^{2+}	Dynamic range	Hill coefficient	pK_a (Ca^{2+} ±)	Ca^{2+}-responsive elements	Fluorophore	Excitation peak (nm)	Emission peak (nm)	Reference
	2mt8YC2.3	FRET	2× COX VIII	1.24 μM	—	—	—	CaM, M13	EGFP, EYFP variant	433	475, 527	(13)
	2mtD1cpv	FRET	2× COX VIII	—	—	—	—	CaM, M13	ECFP, cpVenus	433	475, 528	(16)
	2mtD2cpv	FRET	2× COX VIII	0.097, 7.67 μM	5.3	1.34, 0.77	—	CaM, M13	ECFP, cpVenus	433	475, 528	(91)
	2mtD3cpv	FRET	2× COX VIII	760 nM	5.1	0.74	—	CaM, M13	ECFP, cpVenus	433	475, 528	(91)
	2mtD4cpv	FRET	2× COX VIII	49.68 μM	3.8	1.35	—	CaM, M13	ECFP, cpVenus	433	475, 528	(91)
	4mtD1cpv	FRET	4× COX VIII	—	—	—	—	CaM, M13	ECFP, cpVenus	433	475, 528	(92)
	4mtD3cpv	FRET	4× COX VIII	760 nM	5.1	0.74	—	CaM, M13	ECFP, cpVenus	433	475, 528	(14)
	4mtD1GO-Cam	FRET	4× COX VIII	1.53 μM	—	—	—	CaM, M13	cpEGFP, mKOκ	477	510, 560	(93)
	GCaMP2-mt	Intensio	1× COX VIII	124 nM[b]	—	1.6[b]	—	CaM, M13	cpEGFP	491	516	(94)
	CEPIA2mt	Intensio	2× COX VIII	160 nM[b]	1.7[b]	—	—	CaM, M13	cpEGFP	487	508	(24)
	CEPIA3mt	Intensio	2× COX VIII	11 μM[b]	1.6[b]	—	—	CaM, M13	cpEGFP	487	508	(24)
	CEPIA4mt	Intensio	2× COX VIII	56 μM[b]	1.5[b]	—	—	CaM, M13	cpEGFP	487	508	(24)
	mitGC3	Intensio	1× COX VIII	542 nM	12	2.73	6.6/8.73	CaM, M13	cpEGFP	496	513	(95)
	mito-GCaMP5G	Intensio	1× COX VIII	460 nM	45.4	2.46	6.96/9.14	CaM, M13	cpEGFP	497	515	(96)
	mito-GCaMP6s	Intensio	1× COX VIII	144 nM	63.2	2.9	6.20/9.77	CaM, M13	cpEGFP	497	515	(96)
	2mtGCaMP6m	Intensio	2× COX VIII	167 nM	38.1	2.96	6.90/8.68	CaM, M13	cpEGFP	497	515	(46)
	mitochondrial R-GECO1	Intensio	2× COX VIII	482 nM	16	2.06	6.59/8.9	CaM, M13	cpmApple	561	589	(97)
	mito-LAR-GECO1.2	Intensio	1× COX VIII	12 μM	8.7	1.4	5.8, 8.9/9.0	CaM, M13	cpmApple	557	584	(25)
	mito-GEM-GECO1	Ratio	2× COX VIII	340 nM	110	2.94	6.16	CaM, M13	cpEGFP	390	455, 511	(20)
	mtCamgaroo-2	Intensio	1× COX VIII	5.3 μM	7	1.24	—	CaM	cpEYFP variant	490	514	(11)
	2mt8CG2	Intensio	2× COX VIII	5.3 μM	7	1.24	—	CaM	cpEYFP variant	490	514	(13)
	Ratiometric-Pericam-mt	Ratio	1× COX IV	1.7 μM	—	1.1	—	CaM, M13	cpEYFP	415, 494	517	(19)
	mt8PR	FRET	1× COX VIII	1.7 μM	—	1.1	—	CaM, M13	cpEYFP	415, 494	517	(13)
	2mt8PR	FRET	2× COX VIII	1.7 μM	—	1.1	—	CaM, M13	cpEYFP	415, 494	517	(13)
	RP3.1mt	Ratio	1× COX IV	—	—	—	—	CaM, M13	cpEYFP	410, 480	510	(98)
	mt-inverse pericam 2	Intensio	1× COX VIII	80 nM[b]	—	1.4[b]	—	CaM, M13	cpEYFP	503	515	(35)
	Mitycam-E67Q	Intensio	1× COX VIII	255 nM[b]	—	—	—	CaM, M13	cpEYFP	498	515	(99)
	Mitycam-E31Q	Intensio	1× COX VIII	1.8 μM[b]	—	—	—	CaM, M13	cpEYFP	498	515	(48)
	mito-Case12	Intensio	1× COX VIII	1 μM	12	—	7.2	CaM, M13	cpEGFP	491	516	(100)
	mitGAP	Ratio	1× COX VIII	200 nM	—	1	—	Aequorin	GFP variant, Aequorin	403, 470	510	(21)
Mitochondrial outer membrane	N33D1cpv	FRET	N33 of TOM20	—	—	—	—	CaM, M13	ECFP, cpVenus	433	475, 528	(16)
	OMM-pcm-ER	Ratio	N30 of mAKAP1	460 nM	—	—	—	CaM, M13	cpEYFP	415, 494	517	(26)
	OMM-pcmD2-ER	Ratio	N30 of mAKAP1	3.14 μM	—	—	—	CaM, M13	cpEYFP	415, 494	517	(26)
Nucleus	Cameleon-2nu	FRET	NLS	1.24 μM	—	—	—	CaM, M13	EBFP, EGFP	380	460, 507	(9)
	H2BD1cpv	FRET	Histone 2B	—	—	—	—	CaM, M13	ECFP, cpVenus	433	475, 528	(16)
	CaYang1NLS	FRET	NLS	1.04, 66.8 μM	—	—	—	CaM, M13	mTFP1, mCitrine	462	492, 529	(57)
	NLS-GCaMP2	Intensio	NLS	146 nM	—	3.8	—	CaM, M13	cpEGFP	487	508	(56)
	NLS-R-GECO1	Intensio	NLS	482 nM	16	2.06	6.59/8.9	CaM, M13	cpmApple	561	589	(20)

(*Continued on next page*)

Table 1. *Continued*

Locus	Name	Type[a]	Tag	K_d for Ca^{2+}	Dynamic range	Hill coefficient	pK_a (Ca^{2+} ±)	Ca^{2+}-responsive elements	Fluorophore	Excitation peak (nm)	Emission peak (nm)	Reference
	Ratiometric-pericam-nu	Ratio	NLS	1.7 μM	—	1.1	—	CaM, M13	cpEYFP	415, 494	517	(19)
	nucGAP	Ratio	Nucleoplasmin	200 nM	—	1	—	Aequorin	GFP variant, Aequorin	403, 470	510	(21)
Peroxisomes	D3cpv-KVK-SKL	FRET	KVK-SKL	1 μM	—	—	—	CaM, M13	ECFP, cpVenus	433	475, 528	(15)
Plasma membrane	$P2X_2$-cam	FRET	$P2X_2$	3.98 μM	—	—	—	CaM, M13	EGFP, EYFP variant	433	475, 527	(10)
	Cav2.2-TN-XL	FRET	Cav2.2	2.5 μM	1.7	—	—	Troponin C	CFP, Citrine	432	475, 527	(66)
	Orai-G-GECO1	Intensio	Orai1	749 nM	25	2.97	7.57/10.05	CaM, M13	cpEGFP	496	512	(67)
	Orai-G-GECO1.2	Intensio	Orai1	1.15 μM	23	2.11	7.24/10.44	CaM, M13	cpEGFP	498	513	(67)
Primary cilia	$5HT_6$-G-GECO1.0	Intensio	$5\text{-}HT_6$ receptor	749 nM	25	2.97	7.57/10.05	CaM, M13	cpEGFP	496	512	(28)
	SMO–GCaMP3	Intensio	Smoothened	542 nM	12	2.73	6.6/8.73	CaM, M13	cpEGFP	496	513	(70)
	CTS-G-CaMP3	Intensio	C-tail of fibrocystin	542 nM	12	2.73	6.6/8.73	CaM, M13	cpEGFP	496	513	(72)
	Arl13b-GCaMP5	Intensio	Arl13b	447 nM	45.4	2.46	6.58/8.61	CaM, M13	cpEGFP	496	513	(71)
	Arl13b-GCaMP6	Intensio	Arl13b	144 nM	63.2	2.9	6.20/9.77	CaM, M13	cpEGFP	496	513	(71)

AKAP1, A-kinase anchor protein 1; COX, cytochrome *c* oxidase; NLS, nuclear localization sequences; TOM20, translocase of outer mitochondrial membranes 20 kDA; tPA, tissue plasminogen activator.
[a]Single-FP-type GECIs are classified into two groups: intensiometric (Intensio) and ratiometric (Ratio) indicators.
[b]Measured at pH 8.0.

Although aequorin is a Ca^{2+}-sensitive bioluminescent protein, GAP is a fluorescent indicator and does not require the cofactor coelenterazine. The unique feature of GAP is that it has dual excitation peaks at ~403 and ~470 nm, and a single emission peak at ~510 nm, enabling ratiometric measurements. The ratio of the fluorescence intensity at the two excitation wavelengths increases by 170% upon Ca^{2+} binding. Although it has not been fully understood how GAP detects changes in Ca^{2+} concentration, it is assumed that the aequorin molecule functions as a Ca^{2+}-responsive element inducing a conformational change in the adjacent GFP. The Ca^{2+} affinity of GAP was decreased from a K_d of 200 nM to that of 12 μM by substituting amino acids in the Ca^{2+}-binding sites of aequorin to generate erGAP1.

In addition to the GECIs for intra-ER Ca^{2+} imaging, another type of GECI was developed to visualize Ca^{2+} signals in proximity of the ER membrane. To detect Ca^{2+} release events via the ryanodine receptor Ca^{2+} release channels, GCaMP6f, a GECI for cytosolic Ca^{2+} measurement, was fused with triadin 1 or junctin, which are membrane proteins colocalizing with ryanodine receptor in the junctional regions of the SR in cardiac myocytes. GCaMP6f-T/J were successfully used to visualize Ca^{2+} nanosparks, which are ~50 times smaller in volume than conventional Ca^{2+} sparks (29).

Acidic organelles

Similar to the ER, acidic organelles such as the Golgi apparatus (pH ≈ 6.0–6.7), endosomes (pH ≈ 5.5–6.5), and secretory granules (pH ≈ 5.5) engage in intracellular Ca^{2+} signaling by acting as Ca^{2+} sources (40,41). Ca^{2+} is also thought to be important in the functioning of these acidic organelles, but it remains challenging to visualize Ca^{2+} signals in these organelles with fluorescent indicators because of their acidic environment, which often reduces the brightness of fluorescent indicators.

The first fluorescent GECI specifically developed for acidic organelles was GT-YC3.3 for the Golgi apparatus (11). GT-YC3.3 is a cameleon-type FRET indicator, in which YFP is replaced by a less pH-sensitive EYFP variant, Citrine. GT-YC3.3 was targeted to the Golgi by incorporating the N-terminal sequence of type II galactosyltransferase, and was used to successfully detect Ca^{2+} release from the Golgi upon depletion of the luminal Ca^{2+} with ionomycin, a Ca^{2+} ionophore, although its affinity to Ca^{2+} (K_d = 1.5 μM) appears rather high for Golgi Ca^{2+} concentrations. Later, cameleon-type Golgi GECIs with lower Ca^{2+} affinities were developed: Go-D1cpv and medial Go-D1cpv localized in the *trans* and medial Golgi through incorporation of the N-terminal sequence of sialyl-transferase I and 1,6 *n*-acetyl glucosaminyl transferase, respectively (42,43). These indicators showed that Ca^{2+} uptake into the Golgi depends on both secretory pathway Ca^{2+}

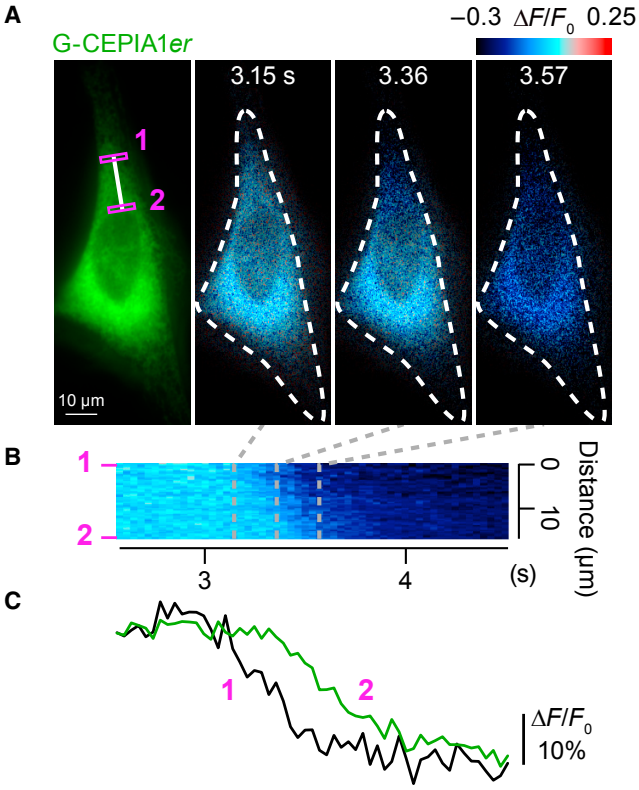

FIGURE 2 High spatiotemporal resolution of ER Ca^{2+} release using CEPIA. (*A*) Time-lapse images of a wavelike decrease in the ER Ca^{2+} concentration in a HeLa cell visualized with G-CEPIA1*er*. Perfusion of 10 μM histamine is started at 0 s. (*B*) Time-course of ER Ca^{2+} dynamics along the white line indicated in (*A*). (*C*) Comparison of ER Ca^{2+} dynamics in the two regions of interest indicated in (*A*). The fluorescence intensity is normalized by the initial intensity. These results show that Ca^{2+} release from the ER initiates at the tips of cells, and then it propagates to the perinuclear region. (*Black line*) Region 1; (*green line*) region 2. This figure is adapted from Suzuki et al. (24). To see this figure in color, go online.

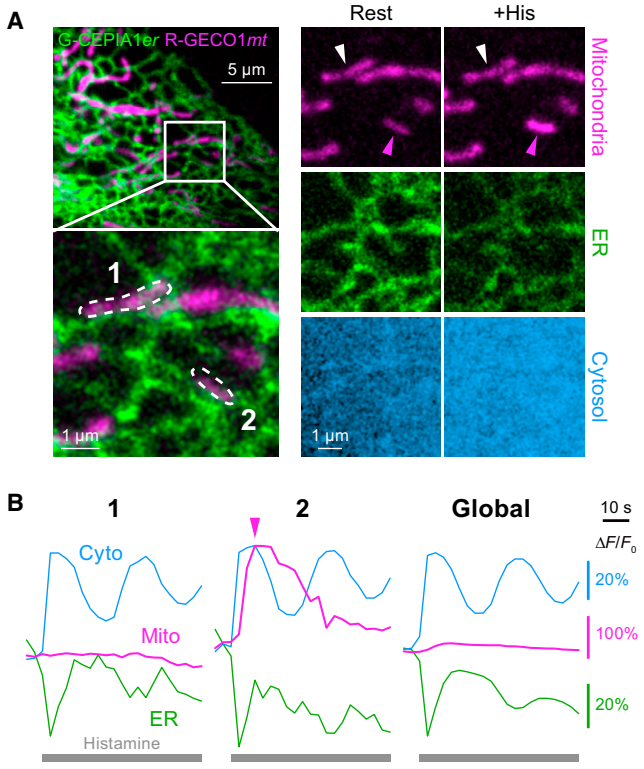

FIGURE 3 Simultaneous imaging of Ca^{2+} signal in three subcellular compartments. (*A*) Ca^{2+} response of a HeLa cell in the resting state (*upper*) and after 10 μM histamine application (*lower*) in the mitochondria (*left*), ER (*middle*), and cytosol (*right*) visualized with R-GECO1*mt*, G-CEPIA1*er*, and GEM-GECO1, respectively. (*B*) Time-courses of Ca^{2+} signal in the mitochondria (*magenta*), ER (*green*), and cytosol (*blue*) within or surrounding the two regions of interest indicated in (*A*). These results show that there is a considerable intracellular inhomogeneity in mitochondrial Ca^{2+} signals after agonist-induced Ca^{2+} release from the ER, while homogeneous responses are observed in the cytosol and the ER. This figure is adapted from Suzuki et al. (24). To see this figure in color, go online.

ATPase1 and sarco/endoplasmic reticulum Ca^{2+} ATPase, but their activities are differently regulated between the *trans* and medial Golgi. In addition, these indicators suggest that there is a gradient in luminal Ca^{2+} concentration among the ER, *cis*-Golgi, and *trans*-Golgi (Fig. 1). Recently, a single-FP-type Golgi GECI, goGAP1, was developed by modifying erGAP1 to utilize its low sensitivity to pH (21).

Fluorescent GECIs for visualizing Ca^{2+} signals in the lumen of secretory granules (SGs) and endosomes have also been developed. D1-SG is based on the cameleon-type GECI D1 attached to tissue plasminogen activator, which localizes in the SGs (17). Measurements using D1-SG suggest that a high concentration of Ca^{2+} (~69 μM) is accumulated in the SGs, and that the Orai1 channel on the SG membranes is important for Ca^{2+} release from the SGs. For Ca^{2+} imaging in the endosomes, TiVAMP-GEM-GECO1 was developed by fusing single-FP-type ratiometric indicator GEM-GECO1 with tetanus-insensitive vesicle-associated membrane protein (TiVAMP), a soluble NSF attachment protein receptor protein localized in the endosomes (27). TiVAMP-GEM-GECO1 shows that the luminal Ca^{2+} concentration of the endosomes is maintained at ~2 μM (Fig. 1), and that endosomes take up Ca^{2+} and act as a Ca^{2+} buffer in response to extracellular glucose stimulation in β-cells.

Mitochondria

Mitochondria, which are primarily involved in oxidative metabolism and cell survival, participate in intracellular Ca^{2+} signaling both as modulators and as sensors (4). In response to cytosolic Ca^{2+} elevation via Ca^{2+} release from the ER or to Ca^{2+} influx from the extracellular space, mitochondria take up Ca^{2+} into the matrix and buffer cytosolic Ca^{2+} elevation to prevent intracellular Ca^{2+} overload. Mitochondrial Ca^{2+} is also important for controlling the mitochondrial metabolism itself, because the activities of mitochondrial enzymes for ATP production rely on the mitochondrial Ca^{2+} concentration (44). Abnormal mitochondrial Ca^{2+} dynamics are involved in cell death or

autophagic degradation of the mitochondria, which are implicated in several neurodegenerative diseases (45). Furthermore, loss-of-function mutations in MICU1, one of the regulator proteins of the mitochondrial Ca^{2+} uniporter, cause brain and muscle disorders in humans (46), even though mice lacking mitochondrial Ca^{2+} uniporter exhibit no severe phenotypes (47). Thus, mitochondrial Ca^{2+} is a critical parameter for cell function, and much attention has been paid to the development of mitochondrial fluorescent GECIs.

Selective localization of GECIs in mitochondria can be achieved by attaching a mitochondrial-targeting sequence (MTS) derived from human cytochrome *c* oxidase subunit VIII or cytochrome *c* oxidase subunit IV, to N-terminus of the indicators (10,19). It has been reported that tandem repeats of the MTS enhance the specificity of the localization of these indicators (13). Because the resting Ca^{2+} level in mitochondria is assumed to be $<$100 nM, which is almost equal to that in the cytoplasm (Fig. 1), a number of cytosolic GECIs fused with the MTS have been successfully used to detect mitochondrial Ca^{2+} dynamics. However, Ca^{2+} affinity is an important parameter even for mitochondrial GECIs because mitochondrial Ca^{2+} concentration can reach up to ~100 μM after certain types of stimulation (4) (Fig. 1). To this end, mitochondrial GECIs possessing low Ca^{2+} affinity have been generated by modifying their Ca^{2+}-responsive element (10,14,16,24,25,48).

In addition to these factors, pH sensitivity is another important factor for mitochondrial GECIs. pH in the mitochondrial matrix is estimated at ~8.0 (40), but direct visualization of spatiotemporal pH dynamics using a genetically encoded mitochondrial pH indicator revealed two unique features of mitochondrial matrix pH: (1) an acidification during cytosolic Ca^{2+} elevation by the activation of Ca^{2+}/H^+ transporters and (2) a spontaneous and transient alkalization, named pH flash (49,50). These mitochondrial pH changes have the potential to cause artifactual fluctuations in the fluorescent intensity of pH-sensitive GECIs. This problem may be alleviated by using mitochondrial GECIs with high pH stability (14,21).

Apart from the mitochondrial matrix, GECIs for visualizing Ca^{2+} dynamics in the proximal region surrounding the mitochondrial outer membrane (OMM) have also been created (16,26). Mitochondria form close contacts with the ER, and this ER-mitochondrial junction is presumed to be important for local regulation of mitochondrial function. In fact, GECIs targeted to the mitochondrial matrix have revealed that considerable heterogeneity is observed in mitochondrial Ca^{2+} signals in response to global elevation of cytosolic Ca^{2+} levels via the activation of inositol 1,4,5-trisphosphate receptors (19,24,51). OMM-attached GECIs have been developed by fusion with the OMM-targeting sequence from A-kinase anchor protein 1 or translocase of outer mitochondrial membrane, 20 kDa. These GECIs have shown that the surface of the mitochondria may be exposed to higher Ca^{2+} concentrations than that of the bulk cytosol in response to Ca^{2+} release from the ER (16,26).

Nucleus

Ca^{2+} is one of the key molecules regulating gene transcription. Cytosolic Ca^{2+} elevation activates Ca^{2+}-sensitive kinases or phosphatases in the cytoplasm and induces translocation of transcription factors from the cytoplasm to the nucleus (52). A Ca^{2+} increase in the nucleus also directly enhances gene transcription by deactivating Ca^{2+}-dependent repressors (53). Thus, nuclear Ca^{2+} dynamics has gathered much attention. Because Ca^{2+} concentrations in the nucleus are assumed to be similar to that in the cytosol (Fig. 1), nuclear GECIs can be generated by attaching nuclear localization sequences to cytosolic GECIs. Actually, a variety of fluorescent indicators including FRET-type and single-FP-type GECIs have been used to visualize nuclear Ca^{2+} signals, showing that the nuclear Ca^{2+} signal is mostly synchronized with the cytosolic Ca^{2+} signal (9,16,19,21,54–57).

Peroxisomes

Peroxisomes are multifunctional organelles regulating the oxidation of fatty acids, biosynthesis of lipids, and reduction of reactive oxygen species (58). Similar to other organelles, it is likely that peroxisomes play several roles in intracellular Ca^{2+} handling or that peroxisomal Ca^{2+} regulates enzyme activities. However, little information is currently available on the dynamics and function of Ca^{2+} in peroxisomes. A cameleon-based FRET GECI for peroxisomes was recently developed, named D3cpv-KVK-SKL (15). It is targeted to the peroxisomes by inserting a three-amino-acid positively charged sequence, Lys-Val-Lys (KVK), and a canonical peroxisomal-targeting signal sequence, Ser-Lys-Leu (SKL), at the C-terminus. Measurements using D3cpv-KVK-SKL show that peroxisomal Ca^{2+} increases in response to cytosolic Ca^{2+} increases, suggesting that peroxisomes function as a Ca^{2+} buffer. Further research is required to clarify the regulatory mechanisms and biological roles of peroxisomal Ca^{2+} dynamics.

Subplasmamembrane

In subplasmamembranous domains, Ca^{2+} signals regulate a variety of biological processes, such as vesicular secretion and ion channel modulation (59). Ca^{2+} influx from the extracellular space via Ca^{2+} channels elevates the local Ca^{2+} concentration up to 100 μM beneath the plasma membrane, resulting in the generation of a Ca^{2+} concentration gradient between the vicinity of the plasma membrane and the bulk of the cytosol (60) (Fig. 1). This suggests that Ca^{2+} signals in the subplasmamembranous regions can be

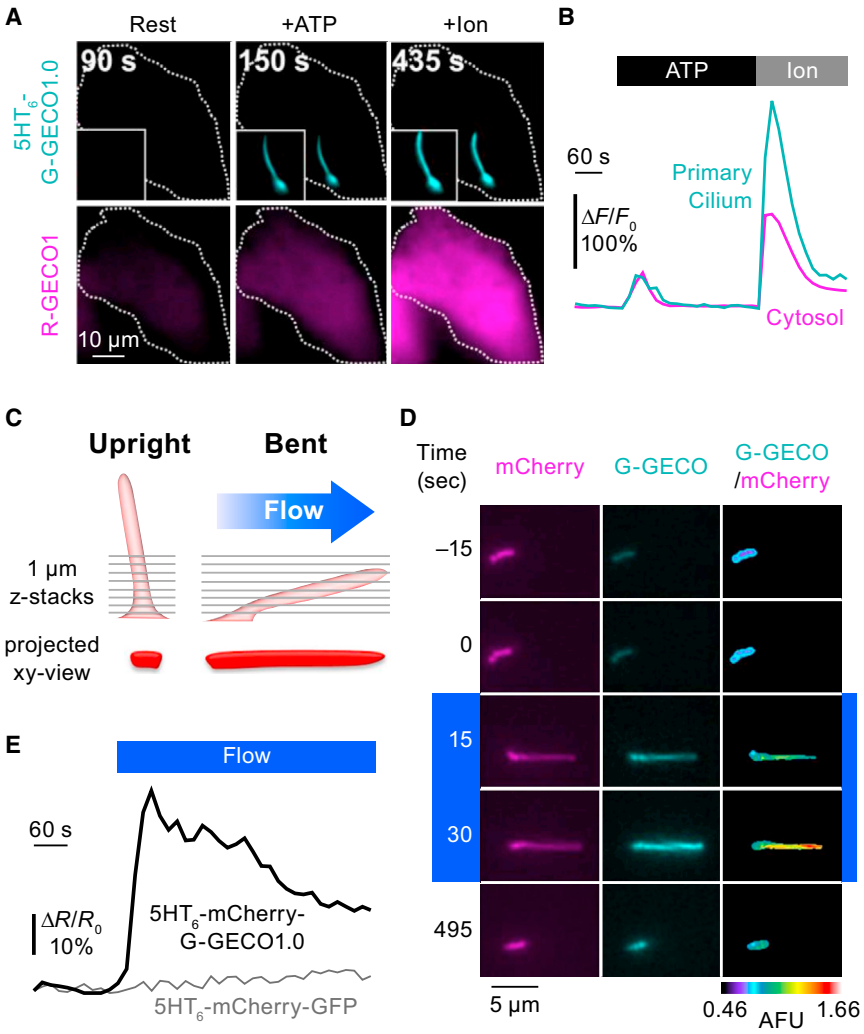

FIGURE 4 Ca^{2+} imaging in the primary cilia upon chemical or mechanical stimulation. (*A*) Ca^{2+} signals in a NIH-3T3 cell in the resting state (*left*), after 10 μM ATP application (*middle*) and after 2 μM ionomycin application (*right*), visualized with 5-HT_6-G-GECO1.0 and R-GECO1 in the primary cilium (*upper*) and the cytosol (*lower*), respectively. (*B*) Time-courses of Ca^{2+} signals in the primary cilium (*cyan*) and cytosol (*magenta*) within the cell indicated in (*A*). (*C*) Schematic of flow-induced movement of a primary cilium. A primary cilium in an upright position bends in response to laminar flow. Images of the primary cilium were generated by z-projections of consecutive *xy*-plane images. (*D*) Time-lapse images of a primary cilium subjected to laminar flow (1 dyne/cm^2 shear, *blue bar*) in a mouse inner medullary collecting duct cell expressing $5HT_6$-mCherry-G-GECO1.0 (*left* and *middle*). mCherry is expressed as a marker to track the spatial movement of the cilium. Time-dependent changes in G-GECO1.0/mCherry fluorescence intensities are shown in pseudo-color (*right*). (*E*) Time-courses of $5HT_6$-mCherry-G-GECO1.0 (*black*) and $5HT_6$-mCherry-GFP (*gray*, as a control). This figure is adapted from Su et al. (28). To see this figure in color, go online.

separately regulated from those in the cytosol. Therefore, the subplasmamembranous domains have been one of the major targets of GECIs, and several types of GECIs have been localized to the plasma membrane by fusion with plasma membrane-anchoring motifs, such as myristoylation, palmitoylation, or farnesylation tags (18,61), or with plasma membrane-localized transporters (62,63). GEGIs fused with synaptic proteins, such as synaptosome-associated protein of 25 kDa (SNAP25), synaptophysin, and synaptobrevin, have been also used to detect microdomain Ca^{2+} signals in the synapse (18,64).

Recently, optical recordings of channel activities on the plasma membrane have been reported, whereby GECIs were localized within close proximity of Ca^{2+} channels by a direct fusion with the channel proteins. $P2X_2$-cam is a purinergic receptor fused with a FRET-type GECI, YC3.1, which successfully detected transmitter-gated Ca^{2+} currents both in vitro and in vivo (65). Another group successfully detected nanodomain Ca^{2+} signals in the surrounding region of $Ca_V2.2$, a voltage-dependent Ca^{2+} channel, by fusion with a FRET-typed GECI, TN-XL (66). A single-FP-typed GECI, G-GECO, was also used by attaching it to Orai1, a Ca^{2+} release-activated Ca^{2+} channel on the plasma membrane, and results from studies with G-GECO revealed that Ca^{2+} influx through Orai1 makes several characteristic patterns, such as rapid transients and periodic oscillation (67).

Primary cilia

A primary cilium is a solitary hairlike organelle on the cell surface that functions as a sensor for diverse chemical and mechanical stimuli (68,69). Emerging evidence suggests that Ca^{2+} acts as a principal second messenger in the signaling pathway in cilia. However, it has been difficult to selectively visualize ciliary Ca^{2+} signal because of its small volume, which is ~1:10,000 of the total cell volume. Recently, four types of ciliary GECIs were created by fusing single-FP-type cytosolic GECIs with ciliary membrane proteins (28,70–72). Ciliary Ca^{2+} imaging with these indicators shows that both stimulation with ATP and laminar fluid flow elicit Ca^{2+} elevation in primary cilia (Fig. 4).

Conclusions and perspectives

Fluorescent GECIs are valuable tools for the measurements of the dynamics and functions of Ca^{2+} signaling in intracellular organelles. Extensive and continuous improvements have made it possible to localize indicators specifically to the desired organelles, to adjust their properties to match the organellar environment, and to resolve the spatiotemporal dynamics of organellar Ca^{2+} signals. However, the currently available organellar GECIs still have several limitations, one of which is in the selection of a signal sequence. As discussed above, the selective and efficient localization of GECIs with organelle-specific targeting sequences is one of the major advantages in their use to image intraorganellar Ca^{2+}, but the organelle-targeting efficiency is affected by several factors. Filippin et al. (13) evaluated the targeting efficiency of mitochondrial targeting sequences in several types of GECIs, and they pointed out that the expression level and maturation speed of GECIs are critical for their targeting efficiency. They also showed that the localization efficiency depends on which GECIs are fused, even when the same signal sequence is used. Additionally, the properties of GECIs, such as Ca^{2+} affinity, can be altered by the signal sequence. Therefore, when imaging intraorganellar Ca^{2+} with GECIs, it is indispensable to carefully evaluate whether the attached signal sequence effectively works for their specific localization in the desired organelle. In situ Ca^{2+} titration of organellar GECIs would be also useful to confirm whether GECIs targeted in the organelle retain the properties, that were measured in vitro, such as K_d and dynamic range.

The kinetics of indicators is also a critical parameter for the further improvement of organellar GECIs. Some types of Ca^{2+} signals—for example, the local Ca^{2+} concentration in the subplasmamembrane domain—can rise and fall within a millisecond. However, GECIs generally exhibit slow kinetics, which limit the detection of such fast Ca^{2+} responses. Much effort has been dedicated to creating cytosolic GECIs that can resolve fast Ca^{2+} signals, especially Ca^{2+} responses generated by action potentials in neurons. Similarly, intraorganellar GECIs with relatively fast kinetics have been developed by several groups. One is CatchER, which successfully detects repetitive Ca^{2+} release from the SR in muscle fibers. G-CEPIA1*er* and R-CEPIA1*er* also exhibit fast kinetics, which can resolve wavelike propagations of ER Ca^{2+} release (Fig. 2). To clarify whether there are any fast Ca^{2+} signals in other organelles and if fast Ca^{2+} signals play any physiological role in organellar functions, further improvement of the kinetics of organellar GECIs will be required.

Another limitation of organellar GECIs is associated with in vivo imaging. Needless to say, in vivo imaging is necessary to fully understand the biological functions of organellar Ca^{2+} signals. However, as compared with imaging in culture dishes, in vivo Ca^{2+} imaging has several technical difficulties, such as severe light scattering by tissues and motion artifacts. Whereas GECIs are now widely used for in vivo cytosolic Ca^{2+} imaging, especially in neuronal cells (73), in vivo organellar Ca^{2+} imaging with GECIs has so far been limited to the ER and mitochondria in zebrafish or mouse skeletal muscles (74–77), possibly due to problems in brightness, signal/noise, kinetics, or affinity for Ca^{2+}. Undoubtedly, improvements in the performance of GECIs, including brightness, dynamic range, kinetics, and affinity, are indispensable to advance the frontiers of in vivo organellar Ca^{2+} imaging. Ratiometric imaging with FRET-typed GECIs may have an advantage in in vivo imaging because it is able to cancel out movement artifacts. At the same time, there are additional promising strategies. One such strategy is the use of near-infrared FPs such as IFP1.4 and iRFP that emit light over 650 nm, which penetrates biological tissues, although these indicators currently require the addition of exogenous biliverdin to obtain bright fluorescent signals (78–80). An alternative strategy is the use of bright LP-based GECIs such as BRAC and nano-lantern (Ca^{2+}) (81–83). These comprise three components: a Ca^{2+}-responsive element, a FP and a LP. Using the process of bioluminescence resonance energy transfer between the LP and the FP, these indicators have successfully detected cytosolic Ca^{2+} dynamics at single-cell resolution, although continuous supply of the cofactor is required to obtain bright images.

The imaging tools discussed above have provided us with useful information on organellar Ca^{2+} dynamics. Additionally, a method allowing organellar-specific manipulation of Ca^{2+} signals will promote research on intraorganellar Ca^{2+} signals. Caged Ca^{2+} compounds, which release Ca^{2+} upon irradiation of UV light, were first used to manipulate intracellular Ca^{2+} signals (84). However, it is difficult to localize caged Ca^{2+} within specific organelles. Recently, several groups successfully generated optogenetic manipulators of cytosolic Ca^{2+} concentrations. One of them is based on a photoactivatable Ca^{2+} releasing protein, named PACR, which is a fusion protein of CaM, M13, and a photosensitive protein, LOV2 (85). Light irradiation changes its conformation and affinity for Ca^{2+}, resulting in release of Ca^{2+}. The others are LOVS1K, OptoSTIM1, and Opto-CRAC, all of which utilize light-dependent activation of the Ca^{2+} channel Orai1 on the plasma membrane, although there are differences among their activation mechanisms (86–88). At present, these methods are used only in the regulation of cytosolic Ca^{2+} concentrations, and none of them have been successfully used in manipulating intraorganellar Ca^{2+} concentrations. Development of methods to control intraorganellar Ca^{2+} levels in a specific and reversible manner would be useful.

Thus, further development of GECIs and genetically encoded Ca^{2+} manipulators are expected to advance our understanding of the functions and roles of organellar Ca^{2+} signals in health and disease.

AUTHOR CONTRIBUTIONS

J.S., K.K., and M.I. wrote the article.

ACKNOWLEDGMENTS

This work was supported by grants from the Ministry of Education, Culture, Sports, Science and Technology, Japan (Nos. 21229004, 25221304, and 25117002 to M.I.; No. 15H05648 to K.K.), and the Takeda Science Foundation to J.S.

REFERENCES

1. Berridge, M. J., P. Lipp, and M. D. Bootman. 2000. The versatility and universality of calcium signalling. *Nat. Rev. Mol. Cell Biol.* 1:11–21.
2. Berridge, M. J., M. D. Bootman, and H. L. Roderick. 2003. Calcium signalling: dynamics, homeostasis and remodelling. *Nat. Rev. Mol. Cell Biol.* 4:517–529.
3. Mekahli, D., G. Bultynck, …, L. Missiaen. 2011. Endoplasmic-reticulum calcium depletion and disease. *Cold Spring Harb. Perspect. Biol.* 3:3.
4. Rizzuto, R., D. De Stefani, …, C. Mammucari. 2012. Mitochondria as sensors and regulators of calcium signalling. *Nat. Rev. Mol. Cell Biol.* 13:566–578.
5. Takahashi, A., P. Camacho, …, B. Herman. 1999. Measurement of intracellular calcium. *Physiol. Rev.* 79:1089–1125.
6. Kendall, J. M., R. L. Dormer, and A. K. Campbell. 1992. Targeting aequorin to the endoplasmic reticulum of living cells. *Biochem. Biophys. Res. Commun.* 189:1008–1016.
7. Rizzuto, R., A. W. Simpson, …, T. Pozzan. 1992. Rapid changes of mitochondrial Ca^{2+} revealed by specifically targeted recombinant aequorin. *Nature.* 358:325–327.
8. Bonora, M., C. Giorgi, …, P. Pinton. 2013. Subcellular calcium measurements in mammalian cells using jellyfish photoprotein aequorin-based probes. *Nat. Protoc.* 8:2105–2118.
9. Miyawaki, A., J. Llopis, …, R. Y. Tsien. 1997. Fluorescent indicators for Ca^{2+} based on green fluorescent proteins and calmodulin. *Nature.* 388:882–887.
10. Arnaudeau, S., W. L. Kelley, …, N. Demaurex. 2001. Mitochondria recycle Ca^{2+} to the endoplasmic reticulum and prevent the depletion of neighboring endoplasmic reticulum regions. *J. Biol. Chem.* 276:29430–29439.
11. Griesbeck, O., G. S. Baird, …, R. Y. Tsien. 2001. Reducing the environmental sensitivity of yellow fluorescent protein. Mechanism and applications. *J. Biol. Chem.* 276:29188–29194.
12. Palmer, A. E., C. Jin, …, R. Y. Tsien. 2004. Bcl-2-mediated alterations in endoplasmic reticulum Ca^{2+} analyzed with an improved genetically encoded fluorescent sensor. *Proc. Natl. Acad. Sci. USA.* 101:17404–17409.
13. Filippin, L., M. C. Abad, …, T. Pozzan. 2005. Improved strategies for the delivery of GFP-based Ca^{2+} sensors into the mitochondrial matrix. *Cell Calcium.* 37:129–136.
14. Palmer, A. E., M. Giacomello, …, R. Y. Tsien. 2006. Ca^{2+} indicators based on computationally redesigned calmodulin-peptide pairs. *Chem. Biol.* 13:521–530.
15. Drago, I., M. Giacomello, …, T. Pozzan. 2008. Calcium dynamics in the peroxisomal lumen of living cells. *J. Biol. Chem.* 283:14384–14390.
16. Giacomello, M., I. Drago, …, T. Pozzan. 2010. Ca^{2+} hot spots on the mitochondrial surface are generated by Ca^{2+} mobilization from stores, but not by activation of store-operated Ca^{2+} channels. *Mol. Cell.* 38:280–290.
17. Dickson, E. J., J. G. Duman, …, B. Hille. 2012. Orai-STIM-mediated Ca^{2+} release from secretory granules revealed by a targeted Ca^{2+} and pH probe. *Proc. Natl. Acad. Sci. USA.* 109:E3539–E3548.
18. Heim, N., and O. Griesbeck. 2004. Genetically encoded indicators of cellular calcium dynamics based on troponin C and green fluorescent protein. *J. Biol. Chem.* 279:14280–14286.
19. Nagai, T., A. Sawano, …, A. Miyawaki. 2001. Circularly permuted green fluorescent proteins engineered to sense Ca^{2+}. *Proc. Natl. Acad. Sci. USA.* 98:3197–3202.
20. Zhao, Y., S. Araki, …, R. E. Campbell. 2011. An expanded palette of genetically encoded Ca^{2+} indicators. *Science.* 333:1888–1891.
21. Rodriguez-Garcia, A., J. Rojo-Ruiz, …, M. T. Alonso. 2014. GAP, an aequorin-based fluorescent indicator for imaging Ca^{2+} in organelles. *Proc. Natl. Acad. Sci. USA.* 111:2584–2589.
22. Wu, J., A. S. Abdelfattah, …, R. E. Campbell. 2014. A long Stokes shift red fluorescent Ca^{2+} indicator protein for two-photon and ratiometric imaging. *Nat. Commun.* 5:5262.
23. Tang, S., H. C. Wong, …, J. J. Yang. 2011. Design and application of a class of sensors to monitor Ca^{2+} dynamics in high Ca^{2+} concentration cellular compartments. *Proc. Natl. Acad. Sci. USA.* 108:16265–16270.
24. Suzuki, J., K. Kanemaru, …, M. Iino. 2014. Imaging intraorganellar Ca^{2+} at subcellular resolution using CEPIA. *Nat. Commun.* 5:4153.
25. Wu, J., D. L. Prole, …, R. E. Campbell. 2014. Red fluorescent genetically encoded Ca^{2+} indicators for use in mitochondria and endoplasmic reticulum. *Biochem. J.* 464:13–22.
26. Csordás, G., P. Várnai, …, G. Hajnóczky. 2010. Imaging interorganelle contacts and local calcium dynamics at the ER-mitochondrial interface. *Mol. Cell.* 39:121–132.
27. Albrecht, T., Y. Zhao, …, J. D. Johnson. 2015. Fluorescent biosensors illuminate calcium levels within defined β-cell endosome subpopulations. *Cell Calcium.* 57:263–274.
28. Su, S., S. C. Phua, …, T. Inoue. 2013. Genetically encoded calcium indicator illuminates calcium dynamics in primary cilia. *Nat. Methods.* 10:1105–1107.
29. Shang, W., F. Lu, …, H. Cheng. 2014. Imaging Ca^{2+} nanosparks in heart with a new targeted biosensor. *Circ. Res.* 114:412–420.
30. Shigetomi, E., S. Kracun, and B. S. Khakh. 2010. Monitoring astrocyte calcium microdomains with improved membrane targeted GCaMP reporters. *Neuron Glia Biol.* 6:183–191.
31. Prins, D., and M. Michalak. 2011. Organellar calcium buffers. *Cold Spring Harb. Perspect. Biol.* 3:3.
32. Henderson, M. J., H. A. Baldwin, …, B. K. Harvey. 2015. A low affinity GCaMP3 variant (GCaMPer) for imaging the endoplasmic reticulum calcium store. *PLoS One.* 10:e0139273.
33. Zou, J., A. M. Hofer, …, J. J. Yang. 2007. Developing sensors for real-time measurement of high Ca^{2+} concentrations. *Biochemistry.* 46:12275–12288.
34. Osibow, K., R. Malli, …, W. F. Graier. 2006. A new type of non-Ca^{2+}-buffering Apo_a-based fluorescent indicator for intraluminal Ca^{2+} in the endoplasmic reticulum. *J. Biol. Chem.* 281:5017–5025.
35. Ishii, K., K. Hirose, and M. Iino. 2006. Ca^{2+} shuttling between endoplasmic reticulum and mitochondria underlying Ca^{2+} oscillations. *EMBO Rep.* 7:390–396.
36. Ravier, M. A., D. Daro, …, P. Gilon. 2011. Mechanisms of control of the free Ca^{2+} concentration in the endoplasmic reticulum of mouse pancreatic β-cells: interplay with cell metabolism and $[Ca^{2+}]_c$ and role of SERCA2b and SERCA3. *Diabetes.* 60:2533–2545.
37. Waldeck-Weiermair, M., H. Bischof, …, R. Malli. 2015. Generation of red-shifted cameleons for imaging Ca^{2+} dynamics of the endoplasmic reticulum. *Sensors (Basel).* 15:13052–13068.
38. Okubo, Y., J. Suzuki, …, M. Iino. 2015. Visualization of mechanisms for depletion and filling of Ca^{2+} within the endoplasmic reticulum upon synaptic inputs in cerebellar Purkinje cells. *J. Neurosci.* 35:15837–15846.

39. Murayama, T., N. Kurebayashi, …, T. Sakurai. 2015. Divergent activity profiles of Type 1 ryanodine receptor channels carrying malignant hyperthermia and central core disease mutations in the amino-terminal region. *PLoS One.* 10:e0130606.

40. Casey, J. R., S. Grinstein, and J. Orlowski. 2010. Sensors and regulators of intracellular pH. *Nat. Rev. Mol. Cell Biol.* 11:50–61.

41. Pinton, P., T. Pozzan, and R. Rizzuto. 1998. The Golgi apparatus is an inositol 1,4,5-trisphosphate-sensitive Ca^{2+} store, with functional properties distinct from those of the endoplasmic reticulum. *EMBO J.* 17:5298–5308.

42. Lissandron, V., P. Podini, …, T. Pozzan. 2010. Unique characteristics of Ca^{2+} homeostasis of the trans-Golgi compartment. *Proc. Natl. Acad. Sci. USA.* 107:9198–9203.

43. Wong, A. K., P. Capitanio, …, P. Pizzo. 2013. Heterogeneity of Ca^{2+} handling among and within Golgi compartments. *J. Mol. Cell Biol.* 5:266–276.

44. McCormack, J. G., A. P. Halestrap, and R. M. Denton. 1990. Role of calcium ions in regulation of mammalian intramitochondrial metabolism. *Physiol. Rev.* 70:391–425.

45. Sheng, Z. H., and Q. Cai. 2012. Mitochondrial transport in neurons: impact on synaptic homeostasis and neurodegeneration. *Nat. Rev. Neurosci.* 13:77–93.

46. Logan, C. V., G. Szabadkai, …, E. Sheridan. 2014. Loss-of-function mutations in MICU1 cause a brain and muscle disorder linked to primary alterations in mitochondrial calcium signaling. *Nat. Genet.* 46:188–193.

47. Pan, X., J. Liu, …, T. Finkel. 2013. The physiological role of mitochondrial calcium revealed by mice lacking the mitochondrial calcium uniporter. *Nat. Cell Biol.* 15:1464–1472.

48. Haviland, S., L. Cleemann, …, M. Morad. 2014. Diversity of mitochondrial Ca^{2+} signaling in rat neonatal cardiomyocytes: evidence from a genetically directed Ca^{2+} probe, mitycam-E31Q. *Cell Calcium.* 56:133–146.

49. Santo-Domingo, J., M. Giacomello, …, N. Demaurex. 2013. OPA1 promotes pH flashes that spread between contiguous mitochondria without matrix protein exchange. *EMBO J.* 32:1927–1940.

50. Poburko, D., J. Santo-Domingo, and N. Demaurex. 2011. Dynamic regulation of the mitochondrial proton gradient during cytosolic calcium elevations. *J. Biol. Chem.* 286:11672–11684.

51. Collins, T. J., P. Lipp, …, M. D. Bootman. 2001. Mitochondrial Ca^{2+} uptake depends on the spatial and temporal profile of cytosolic Ca^{2+} signals. *J. Biol. Chem.* 276:26411–26420.

52. Mellström, B., M. Savignac, …, J. R. Naranjo. 2008. Ca^{2+}-operated transcriptional networks: molecular mechanisms and in vivo models. *Physiol. Rev.* 88:421–449.

53. Carrión, A. M., W. A. Link, …, J. R. Naranjo. 1999. DREAM is a Ca^{2+}-regulated transcriptional repressor. *Nature.* 398:80–84.

54. Ikeda, M., T. Sugiyama, …, C. N. Allen. 2003. Circadian dynamics of cytosolic and nuclear Ca^{2+} in single suprachiasmatic nucleus neurons. *Neuron.* 38:253–263.

55. Robert, V., P. Gurlini, …, T. Pozzan. 2001. Beat-to-beat oscillations of mitochondrial $[Ca^{2+}]$ in cardiac cells. *EMBO J.* 20:4998–5007.

56. Bengtson, C. P., H. E. Freitag, …, H. Bading. 2010. Nuclear calcium sensors reveal that repetition of trains of synaptic stimuli boosts nuclear calcium signaling in CA1 pyramidal neurons. *Biophys. J.* 99:4066–4077.

57. Ding, Y., H. W. Ai, …, R. E. Campbell. 2011. Förster resonance energy transfer-based biosensors for multiparameter ratiometric imaging of Ca^{2+} dynamics and caspase-3 activity in single cells. *Anal. Chem.* 83:9687–9693.

58. Lodhi, I. J., and C. F. Semenkovich. 2014. Peroxisomes: a nexus for lipid metabolism and cellular signaling. *Cell Metab.* 19:380–392.

59. Tovey, S. C., P. de Smet, …, M. D. Bootman. 2001. Calcium puffs are generic $InsP_3$-activated elementary calcium signals and are downregulated by prolonged hormonal stimulation to inhibit cellular calcium responses. *J. Cell Sci.* 114:3979–3989.

60. Rizzuto, R., and T. Pozzan. 2006. Microdomains of intracellular Ca^{2+}: molecular determinants and functional consequences. *Physiol. Rev.* 86:369–408.

61. Shigetomi, E., S. Kracun, …, B. S. Khakh. 2010. A genetically targeted optical sensor to monitor calcium signals in astrocyte processes. *Nat. Neurosci.* 13:759–766.

62. Lee, M. Y., H. Song, …, M. P. Blaustein. 2006. Local subplasma membrane Ca^{2+} signals detected by a tethered Ca^{2+} sensor. *Proc. Natl. Acad. Sci. USA.* 103:13232–13237.

63. Mohamed, T. M., R. Abou-Leisa, …, D. Oceandy. 2013. Development and characterization of a novel fluorescent indicator protein PMCA4-GCaMP2 in cardiomyocytes. *J. Mol. Cell. Cardiol.* 63:57–68.

64. Pinton, P., T. Tsuboi, …, G. A. Rutter. 2002. Dynamics of glucose-induced membrane recruitment of protein kinase C β II in living pancreatic islet β-cells. *J. Biol. Chem.* 277:37702–37710.

65. Richler, E., S. Chaumont, …, B. S. Khakh. 2008. Tracking transmitter-gated P2X cation channel activation in vitro and in vivo. *Nat. Methods.* 5:87–93.

66. Tay, L. H., I. E. Dick, …, D. T. Yue. 2012. Nanodomain Ca^{2+} of Ca^{2+} channels detected by a tethered genetically encoded Ca^{2+} sensor. *Nat. Commun.* 3:778.

67. Dynes, J. L., A. Amcheslavsky, and M. D. Cahalan. 2016. Genetically targeted single-channel optical recording reveals multiple Orai1 gating states and oscillations in calcium influx. *Proc. Natl. Acad. Sci. USA.* 113:440–445.

68. Singla, V., and J. F. Reiter. 2006. The primary cilium as the cell's antenna: signaling at a sensory organelle. *Science.* 313:629–633.

69. Whitfield, J. F. 2008. The solitary (primary) cilium—a mechanosensory toggle switch in bone and cartilage cells. *Cell. Signal.* 20:1019–1024.

70. Delling, M., P. G. DeCaen, …, D. E. Clapham. 2013. Primary cilia are specialized calcium signalling organelles. *Nature.* 504:311–314.

71. Yuan, S., L. Zhao, …, Z. Sun. 2015. Intraciliary calcium oscillations initiate vertebrate left-right asymmetry. *Curr. Biol.* 25:556–567.

72. Jin, X., A. M. Mohieldin, …, S. M. Nauli. 2014. Cilioplasm is a cellular compartment for calcium signaling in response to mechanical and chemical stimuli. *Cell. Mol. Life Sci.* 71:2165–2178.

73. Grienberger, C., and A. Konnerth. 2012. Imaging calcium in neurons. *Neuron.* 73:862–885.

74. Mizuno, H., T. Sassa, …, A. Miyawaki. 2013. Transgenic zebrafish for ratiometric imaging of cytosolic and mitochondrial Ca^{2+} response in teleost embryo. *Cell Calcium.* 54:236–245.

75. Jiménez-Moreno, R., Z. M. Wang, …, O. Delbono. 2010. Sarcoplasmic reticulum Ca^{2+} depletion in adult skeletal muscle fibres measured with the biosensor D1ER. *Pflugers Arch.* 459:725–735.

76. Rudolf, R., P. J. Magalhães, and T. Pozzan. 2006. Direct in vivo monitoring of sarcoplasmic reticulum Ca^{2+} and cytosolic cAMP dynamics in mouse skeletal muscle. *J. Cell Biol.* 173:187–193.

77. Rudolf, R., M. Mongillo, …, T. Pozzan. 2004. In vivo monitoring of Ca^{2+} uptake into mitochondria of mouse skeletal muscle during contraction. *J. Cell Biol.* 166:527–536.

78. Filonov, G. S., K. D. Piatkevich, …, V. V. Verkhusha. 2011. Bright and stable near-infrared fluorescent protein for in vivo imaging. *Nat. Biotechnol.* 29:757–761.

79. Yu, D., M. A. Baird, …, X. Shu. 2015. A naturally monomeric infrared fluorescent protein for protein labeling in vivo. *Nat. Methods.* 12:763–765.

80. Lin, L. T., B. S. Wang, …, Y. J. Lee. 2013. mPlum-IFP 1.4 fluorescent fusion protein may display Förster resonance energy transfer associated properties that can be used for near-infrared based reporter gene imaging. *J. Biomed. Opt.* 18:126013.

81. Takai, A., M. Nakano, …, T. Nagai. 2015. Expanded palette of Nanolanterns for real-time multicolor luminescence imaging. *Proc. Natl. Acad. Sci. USA.* 112:4352–4356.

82. Saito, K., Y. F. Chang, …, T. Nagai. 2012. Luminescent proteins for high-speed single-cell and whole-body imaging. *Nat. Commun.* 3:1262.

83. Saito, K., N. Hatsugai, …, T. Nagai. 2010. Auto-luminescent genetically-encoded ratiometric indicator for real-time Ca^{2+} imaging at the single cell level. *PLoS One.* 5:e9935.

84. Ellis-Davies, G. C. 2007. Caged compounds: photorelease technology for control of cellular chemistry and physiology. *Nat. Methods.* 4:619–628.

85. Fukuda, N., T. Matsuda, and T. Nagai. 2014. Optical control of the Ca^{2+} concentration in a live specimen with a genetically encoded Ca^{2+}-releasing molecular tool. *ACS Chem. Biol.* 9:1197–1203.

86. Pham, E., E. Mills, and K. Truong. 2011. A synthetic photoactivated protein to generate local or global Ca^{2+} signals. *Chem. Biol.* 18:880–890.

87. Kyung, T., S. Lee, …, W. D. Heo. 2015. Optogenetic control of endogenous Ca^{2+} channels in vivo. *Nat. Biotechnol.* 33:1092–1096.

88. He, L., Y. Zhang, …, Y. Zhou. 2015. Near-infrared photoactivatable control of Ca^{2+} signaling and optogenetic immunomodulation. *eLife.* 4:4.

89. Ai, H. W., J. N. Henderson, …, R. E. Campbell. 2006. Directed evolution of a monomeric, bright and photostable version of Clavularia cyan fluorescent protein: structural characterization and applications in fluorescence imaging. *Biochem. J.* 400:531–540.

90. Abell, E., R. Ahrends, …, M. N. Teruel. 2011. Parallel adaptive feedback enhances reliability of the Ca^{2+} signaling system. *Proc. Natl. Acad. Sci. USA.* 108:14485–14490.

91. Palmer, A. E., and R. Y. Tsien. 2006. Measuring calcium signaling using genetically targetable fluorescent indicators. *Nat. Protoc.* 1:1057–1065.

92. Zampese, E., C. Fasolato, …, P. Pizzo. 2011. Presenilin 2 modulates endoplasmic reticulum (ER)-mitochondria interactions and Ca^{2+} cross-talk. *Proc. Natl. Acad. Sci. USA.* 108:2777–2782.

93. Waldeck-Weiermair, M., M. R. Alam, …, R. Malli. 2012. Spatiotemporal correlations between cytosolic and mitochondrial Ca^{2+} signals using a novel red-shifted mitochondrial targeted cameleon. *PLoS One.* 7:e45917.

94. Iguchi, M., M. Kato, …, M. Akao. 2012. Direct monitoring of mitochondrial calcium levels in cultured cardiac myocytes using a novel fluorescent indicator protein, GCaMP2-mt. *Int. J. Cardiol.* 158:225–234.

95. Isshiki, M., M. Nishimoto, …, T. Fujita. 2013. FRET-based sensor analysis reveals caveolae are spatially distinct Ca^{2+} stores in endothelial cells. *Cell Calcium.* 54:395–403.

96. Li, H., X. Wang, …, S. Ding. 2014. Imaging of mitochondrial Ca^{2+} dynamics in astrocytes using cell-specific mitochondria-targeted GCaMP5G/6s: mitochondrial Ca^{2+} uptake and cytosolic Ca^{2+} availability via the endoplasmic reticulum store. *Cell Calcium.* 56:457–466.

97. Lynes, E. M., A. Raturi, …, T. Simmen. 2013. Palmitoylation is the switch that assigns calnexin to quality control or ER Ca^{2+} signaling. *J. Cell Sci.* 126:3893–3903.

98. Frieden, M., D. James, …, N. Demaurex. 2004. Ca^{2+} homeostasis during mitochondrial fragmentation and perinuclear clustering induced by hFis1. *J. Biol. Chem.* 279:22704–22714.

99. Kettlewell, S., P. Cabrero, …, G. L. Smith. 2009. Changes of intramitochondrial Ca^{2+} in adult ventricular cardiomyocytes examined using a novel fluorescent Ca^{2+} indicator targeted to mitochondria. *J. Mol. Cell. Cardiol.* 46:891–901.

100. Chang, K. T., R. F. Niescier, and K. T. Min. 2011. Mitochondrial matrix Ca^{2+} as an intrinsic signal regulating mitochondrial motility in axons. *Proc. Natl. Acad. Sci. USA.* 108:15456–15461.